



**HAL**  
open science

## **Amine-terminated silicon nanoparticles: synthesis, optical properties and their use in bioimaging**

Milena Rosso-Vasic, Evan Spruijt, Zoran Popovic, Karin Overgaag, Barend van Lagen, B. Grandidier, Daniel Vanmaekelbergh, David Dominguez-Gutierrez, Luisa de Cola, Han Zuilhof

### ► To cite this version:

Milena Rosso-Vasic, Evan Spruijt, Zoran Popovic, Karin Overgaag, Barend van Lagen, et al.. Amine-terminated silicon nanoparticles: synthesis, optical properties and their use in bioimaging. *Journal of Materials Chemistry*, 2009, 19 (33), pp.5926-5933. 10.1039/b902671a . hal-00473065

**HAL Id: hal-00473065**

**<https://hal.science/hal-00473065>**

Submitted on 9 Jun 2022

**HAL** is a multi-disciplinary open access archive for the deposit and dissemination of scientific research documents, whether they are published or not. The documents may come from teaching and research institutions in France or abroad, or from public or private research centers.

L'archive ouverte pluridisciplinaire **HAL**, est destinée au dépôt et à la diffusion de documents scientifiques de niveau recherche, publiés ou non, émanant des établissements d'enseignement et de recherche français ou étrangers, des laboratoires publics ou privés.



Distributed under a Creative Commons Attribution - NonCommercial 4.0 International License

# Amine-terminated silicon nanoparticles: synthesis, optical properties and their use in bioimaging

Milena Rosso-Vasic,<sup>a</sup> Evan Spruijt,<sup>a</sup> Zoran Popović,<sup>b</sup> Karin Overgaag,<sup>c</sup> Barend van Lagen,<sup>a</sup> Bruno Grandidier,<sup>d</sup> Daniel Vanmaekelbergh,<sup>c</sup> David Domínguez-Gutiérrez,<sup>b</sup> Luisa De Cola<sup>\*b</sup> and Han Zuilhof<sup>†\*a</sup>

Very stable and bright emitting amine-terminated Si nanoparticles (NPs) with different alkyl chain lengths between the Si core and amine end-group are synthesized. The obtained NPs have a spherical shape and homogeneous size distribution ( $1.57 \pm 0.24$  nm). Their emission can be tuned from the UV to the blue spectral region, in a controllable fashion, by only changing the alkyl spacer length. The emission quantum yields are  $\sim 12\%$  for all synthesized Si NPs. Excited state lifetimes are in the ns range and point to a direct band gap excitation.  $\text{NH}_2$ -terminated Si NPs exhibit an exceptional stability over a wide pH range (1–13) and high temperatures (120 °C). The diffusion coefficient of prepared Si NPs is determined by fluorescence correlation spectroscopy (FCS) to be  $3.3 \times 10^{-10} \text{ m}^2 \text{ s}^{-1}$ . The derived size of Si NPs from mobility corresponds to 1.4 nm which is in a good agreement with the size obtained by transmission electron microscopy (TEM). Prepared Si NPs are shown to be highly suitable for bioimaging studies as they are readily taken up by BV2 cells. Si NPs are located in the cells cytosol. Proliferation of stained BV2 cells is observed and showed that newly formed cells are also stained with Si NPs, indicating their minimal toxicity. By using Si NPs it is possible to stain multiple cell generations by only staining the mother cells.

## Introduction

Over the last few years silicon nanoparticles (Si NPs) have attracted a lot of interest because of their exceptional optical properties, such as size-dependent tunable light emission,<sup>1–3</sup> high brightness,<sup>4</sup> and their great stability against photo-bleaching compared to organic dye molecules.<sup>5,6</sup> Moreover, Si exhibits a low inherent toxicity<sup>7</sup> in comparison with the heavy elements of several other types of semiconductor quantum dots.<sup>8–10</sup> The combination of these properties opens up a new avenue of applications of Si NPs for optoelectronic<sup>11</sup> and bioimaging purposes.<sup>12,13</sup>

Free-standing luminescent Si NPs of 1–8 nm size have been produced using a variety of techniques such as: ultrasonic dispersion of electrochemically etched silicon,<sup>14</sup> laser-driven pyrolysis of silane,<sup>15–18</sup> synthesis in supercritical fluids<sup>2,19</sup> and wet chemistry techniques—reduction of Zintl salts in inert organic solvents<sup>20–24</sup> and in micelles using  $\text{SiX}_4$  ( $X = \text{Cl}, \text{Br}$  or  $\text{I}$ ) as a silicon source.<sup>5,6b,25–27</sup> The obtained NPs were halogen-terminated<sup>21,28</sup> or hydrogen-terminated<sup>15,16,29,30</sup> and very prone to oxidation.<sup>31</sup> Therefore, further stabilization is desirable, e.g. by reaction with alkyl-lithium salts<sup>21</sup> or terminal alkenes<sup>32</sup> to

provide Si–C linkages. These passivation methods were similar to those developed for planar<sup>33</sup> or porous<sup>34</sup> silicon, for which the attachment can be initiated thermally,<sup>35,36</sup> or photochemically with UV<sup>37</sup> or visible light.<sup>33a,38–40</sup> Hydrosilylation of Si NPs was also successfully performed by using a variety of platinum-based<sup>5,6b</sup> or triphenylcarbenium-based catalysts.<sup>42</sup>

The light emission of Si nanocrystals has been attributed to the decay of quantum-confined excitons<sup>43</sup> as well as decay mechanisms mediated by surface atoms.<sup>44,45</sup> The exciton can be self-trapped or luminescence can occur *via* an energy level located in the band gap,<sup>46</sup> or *via* energy transfer to a covalently attached dye with a suitable excitation energy.<sup>41</sup> Quantum confinement is controlled by the size of the core of the NPs, but full control over the surface properties is also important in order to achieve desirable emission characteristics, which itself requires improved methods for producing well-defined NPs. Indeed, changing the capping group of Si NPs can significantly shift the emission energy. A direct comparison of the emissions of alkyl- and amine-terminated Si NPs of the same size displays a significant red shift for the amine-terminated NPs.<sup>27,41</sup> Interestingly, the emission of  $\text{NH}_2$ -terminated NPs was intense, despite the presence of  $\text{NH}_2$  moieties. This contrasts with observations of CdSe NPs, the emission of which is strongly quenched when an amine group is present in the solvent, in the form of an alkylamine.<sup>47,48</sup>

The ability to make NPs water-soluble and to target them to specific biomolecules using proper anchors as capping groups has led to promising applications in cellular and assay labelling techniques, as well as in deep-tissue imaging.<sup>49–52</sup> For such purposes core–shell–coating NPs (e.g. CdSe–ZnS–silane NPs) have been studied the most so far.<sup>53–55</sup> Despite their wide absorption and emission range (from UV to IR) and their

<sup>a</sup>Laboratory of Organic Chemistry, Wageningen University, Dreijenplein 8, 6703 HB Wageningen, The Netherlands. E-mail: Han.Zuilhof@wur.nl; Fax: +31-317-484914; Tel: +31-317-482367

<sup>b</sup>Physikalisches Institut, and CeNTech, Westfälische Wilhelms-Universität Münster, Mendelstrasse, D-48149 Münster, Germany. E-mail: decola@uni-muenster.de; Fax: +49 (0)251/980-2834; Tel: +49 (0)251/980-2873

<sup>c</sup>Debye Institute for Nanomaterial Science, Utrecht University, Princetonplein 1, 3508 TH Utrecht, The Netherlands

<sup>d</sup>Institut d'Electronique, Microélectronique et de Nanotechnologie (IEMN) (CNRS, UMR 8520), Département ISEN, 41 bd Vauban, 59046 Lille Cedex, France

exceptional brightness there are two main disadvantages that significantly limit their application: large overall size and toxicity. The minimal size of core–shell–coat NPs is 10–20 nm and while the core size is still small enough for quantum confinement phenomena, this overall size greatly restricts their use for cellular applications. In addition, although the silane coating plays an important role in reducing their toxicity, the packing density and porosity of this organic monolayer are hard to control.

Water-soluble Si NPs seem to be good candidates to overcome these drawbacks. Li and Ruckenstein have already demonstrated the possibility of labelling the surface of Chinese hamster ovary (CHO) cells with red-emitting poly(acrylic acid) functionalized Si NPs.<sup>56</sup> More recently, Tilley *et al.* labeled Vero cells with amino-terminated Si NPs, and gave an indication that NPs were probably transfected into the cytosol.<sup>27</sup> However, the uptake and lifecycle of cells labeled with Si NPs have not been published yet.

The aim of our research is twofold: to determine the influence of amine groups and linker lengths on the optical properties of alkylamine-functionalized Si NPs, to determine their band gap and examine their cellular uptake by determining their location inside the cell and the behavior of cells after labelling.

For that purpose we have synthesized hydrogen-terminated Si NPs in reverse micelles, and functionalized them with three different amine-terminated  $\omega$ -alkenes: allylamine, hex-5-en-1-amine and undec-10-en-1-amine. Here we report on the synthesis and photophysics of such species, including both steady-state and time-resolved absorption and emission spectroscopy at various pH values, to determine the effect of the lone pair on the nitrogen of the capping amine group on the optical properties of Si NPs. Furthermore, we have performed ultra-high vacuum (UHV) cryogenic scanning tunneling microscopy (STM) and spectroscopy (STS) on Si NPs, with the aim of providing unique information on the electronic properties of the individual nanocrystals as STS can probe the complete density of states without being limited by selection rules that play a part in optical experiments.<sup>57</sup> In addition, we have experimentally determined the diffusion coefficient of Si NPs, a highly relevant value to predict their mobility in physiological media. Finally, we successfully stained a murine cell line (BV2) with Si NPs and observed the location of NPs inside the cell, and the continued proliferation of cells. This last experiment truly reveals the potential of Si NPs for bioimaging.

## Experimental

All chemicals used were purchased from Sigma-Aldrich and employed without further purification unless specified. Toluene [(H<sub>2</sub>O  $\leq$  0.005%),  $\geq$  99.7% (GC)] was dried over Na wire overnight prior to use. Methanol was distilled and stored on anhydrous MgSO<sub>4</sub>.

### Synthesis of alkeneamines and Si NPs

**Hex-5-en-1-amine.** 6-Bromo-1-hexene (5 ml; 0.04 mol) was dissolved in 50 ml DMF. After addition of NaN<sub>3</sub> (0.20 mol) the mixture was stirred at 35 °C for 24 h. Cold water was added and 6-azido-hex-1-ene was extracted with petroleum ether (PE 40/60) and washed 3 times with brine. Pure 6-azido-hex-1-ene has been obtained with 75% yield. <sup>1</sup>H NMR (300 MHz, CDCl<sub>3</sub>, 293 K):  $\delta$ (ppm) 5.81 (m, 1H), 4.99 (m, 2H), 3.26 (t, 2H), 2.07 (m, 2H), 1.60–1.36 (m, 6H).

NH<sub>4</sub>Cl [0.09 mol, in 120 ml of ethanol–water (3 : 1) mixture] was added to 6-azido-hex-1-ene. Upon addition of 3.4 g of Zn powder, the reaction mixture was refluxed for 30 min. The mixture was filtered and ethanol was evaporated under reduced pressure. 12 ml of aqueous ammonia solution and 120 ml of ethyl acetate were added in order to extract hex-5-enylamine. The amine solution in ethyl acetate was washed 3 times with brine and the solvent was removed under reduced pressure and dried over magnesium sulfate. Pure hex-5-en-1-amine is obtained with 62% yield. <sup>1</sup>H NMR (300 MHz, CDCl<sub>3</sub>, 293 K):  $\delta$ (ppm) 5.81 (m, 1H), 4.98 (m, 2H), 2.71 (t, 2H), 1.40–1.10 (m, 8H).

**Undec-10-en-1-amine.** 11-Bromoundecene-1-ene (10 ml; 0.05 mol) was dissolved in 50 ml of DMF. After addition of NaN<sub>3</sub> (0.20 mol) the mixture was stirred at 90 °C for 24 h. Cold water was added and 11-azidoundec-1-ene was extracted with petroleum ether (PE 40/60) and washed 3 times with brine. Pure 11-azidoundec-1-ene has been obtained with 90.3% yield. <sup>1</sup>H NMR (300 MHz, CDCl<sub>3</sub>, 293 K):  $\delta$ (ppm) 5.80 (m, 1H), 4.99 (m, 2H), 3.26 (t, 2H), 2.09 (m, 2H), 1.61 (m, 2H), 1.39 (m, 12H).

NH<sub>4</sub>Cl [0.14 mol dissolved in 200 ml ethanol–water (3 : 1)] was added to 11-azidoundec-1-ene. Upon addition of 3.9 g of Zn powder, the reaction mixture was refluxed for 30 min. The mixture was filtered and ethanol was evaporated under reduced pressure. 20 ml of aqueous ammonia solution and 200 ml of ethyl acetate were added in order to extract dodec-11-enylamine. The amine solution in ethyl acetate was washed 3 times with brine and the solvent was removed under reduced pressure and dried over magnesium sulfate. Pure undec-10-en-1-amine is obtained with 85% yield. <sup>1</sup>H NMR (300 MHz, CDCl<sub>3</sub>, 293 K):  $\delta$ (ppm) 5.87 (m, 1H), 4.97 (m, 2H), 2.71 (t, 2H), 1.42–1.17 (m, 18H).

**Synthesis of amino-terminated Si NPs.** Silicon nanoparticles (Si NPs) were prepared using our modification<sup>6b</sup> of a method reported by Warner *et al.*<sup>5</sup> 1.5 g of tetraoctylammonium bromide was mixed with 100 ml of dry toluene and the mixture was sonicated for 30 min, under a flow of dry Ar. 100  $\mu$ l of Si(OCH<sub>3</sub>)<sub>4</sub> was added *via* a gas-tight syringe and sonication was continued for 30 min allowing entry into the micelles. Subsequently, 2.3 ml of LiAlH<sub>4</sub> (1 M in THF) was added in order to form hydrogen-terminated Si NPs. After 30 min sonication, dry and deaerated methanol (30 ml) was added to react with the excess LiAlH<sub>4</sub>.

Alkylamine-terminated NPs with three different alkyl chain lengths were obtained in the reactions of degassed allylamine (2.7 g), hex-5-en-1-amine (2.4 g) and undec-10-en-1-amine (4.4 g) to each flask with hydrogen-terminated Si NPs under Ar, in the presence of 40  $\mu$ l of 0.05 M H<sub>2</sub>PtCl<sub>6</sub> catalyst. After 30 min sonication, 3-aminopropyl, 6-aminohexyl and 11-aminododecyl Si NPs were extracted with water, washed with ethyl acetate and filtered twice through syringe membrane filters (Millex, Millipore, PVDF, 0.45  $\mu$ m). The resulting Si NPs were further purified by dialysis against water (MWCO 7000, SERVA, Membra-Cel dialysis tubing, diameter 22 mm) to remove any residual non-reacted aminoalkene and surfactant.

### Optical measurements

All measurements have been performed at standard pressure and room temperature, unless stated differently. Electronic

absorption spectra were recorded in a quartz cuvette (1 cm, Hellma), using a Cary 1 UV-Vis double-beam spectrophotometer and were corrected for the solvent absorption. The scan range was 200–500 nm with a 600 nm min<sup>-1</sup> rate. Vibration peaks were identified from the positions of the negative peaks in the second derivative of the absorption spectra. Steady-state and time-resolved measurements were performed on a time-correlating single photon counting F900 spectrometer (Edinburgh Instruments), with an instrument response function for time-resolved measurements of 87 ps. All steady-state spectra are corrected for the wavelength-dependent sensitivity of the detector and the source by recording reference data simultaneously. Additionally, emission spectra have been corrected for Raman scattering using the solvent emission spectrum.

Using a comparative method by Williams *et al.*,<sup>58</sup> luminescence quantum yields were measured in optically dilute solutions (optical density ~0.1), using 2-aminopyridine in a 0.05 M aqueous solution of sulfuric acid ( $\Phi_{\text{em}} = 0.60$ ) as a reference emitter.

Time-resolved fluorescence measurements were performed with exactly the same solution as used for the steady-state spectra (absorption was always adjusted to be  $\leq 0.5$ ). A pulsed light-emitting diode ( $\lambda_{\text{excitation}} = 372$  nm) was used as excitation source, and photons were collected up to 20 ns (4096 channels) until a maximum of 10<sup>4</sup> counts.

pH values were set to 1.0 by adding trifluoroacetic acid, 7.5 by adding phosphate buffer (75 mM) and pH = 13.6 by adding NaOH in water. For lifetime measurements, the particles are left at each pH for 6 h prior to measurement.

<sup>1</sup>H NMR spectra were recorded on a Bruker AC-E 400 spectrometer in CDCl<sub>3</sub> (dried over Al<sub>2</sub>O<sub>3</sub>).

High-resolution transmission electron microscopy (TEM) studies were performed with a LIBRA 200 FE (200 kV) microscope. TEM samples were prepared by dipping a carbon-coated 300 mesh copper grid into a sonicated and filtered solution of Si NPs in water. The solvent was evaporated in air and TEM micrographs were typically taken at five different spots of each grid. Olympus Soft Imaging iTEM Solution and iTEM Solution EMaker were used to view and analyse the micrographs, respectively.

Fluorescence correlation spectroscopy (FCS) measurements were performed with a Zeiss LSM ConfoCor 2 combined microscope system (Carl Zeiss, Jena, Germany). For the excitation of the Alexa488 and Si NPs, the 457 nm line of an air-cooled argon ion laser was used. The laser power was set at 2.5 microwatts. A solution of Alexa 488 in nanopure water was used for the calibration of the beam profile. The beam radius is determined from the measured diffusion time ( $\tau_D$ ) and the known diffusion coefficient of Alexa 488 ( $D = 2.24 \times 10^{-10}$  m<sup>2</sup> s<sup>-1</sup>). Samples were placed in 8-chambered plates (Nunc, Rochester, NY) with a borosilicate bottom. Autocorrelation traces were acquired 10 times with 30 s periods.

### Scanning tunneling microscopy (STM) and spectroscopy (STS)

A flame-annealed Au(111) substrate was placed in a solution (chloroform) with propylamine-terminated Si NPs for a few min and then thoroughly rinsed before placing it in the set-up. Amine-terminated Si NPs were attached to a Au substrate by

a Au–NH<sub>2</sub> bond. The STM–STS was performed on a UHV cryogenic set-up (OMICRON). Tunneling spectra were acquired at 5 K in a low-temperature STM, by placing the STM tip above the center of an isolated dot well-separated from the neighboring NPs and disconnecting the feedback loop. The tunneling current  $I$  is measured as a function of the tip–substrate potential difference ( $V_{\text{bias}}$ ).<sup>59</sup> Typically, 100 spectra per STS setting were acquired above a single dot and checked for reproducibility. The spectra are acquired at low set-point currents to ensure the experiments were performed in the shell-tunneling regime.<sup>57</sup>

### Cell staining

$2.5 \times 10^5$  cells were suspended in phosphate buffer solution (PBS) and mixed with the NPs (15.3 mg l<sup>-1</sup>) in 1 : 1 ratio. The mixture was incubated at 37 °C for 5 min and the cells were centrifuged. The formed pallet was suspended in 500  $\mu$ l of PBS and analyzed under the microscope in a microwell plate. Cells were observed using a laser scanning confocal microscope Leica TCS SPE through a 100  $\times$  1.30 NA oil immersion objective. The pinhole was set to one Airy. Si NPs were excited using a 488 nm laser. Epifluorescence was recorded with a black and white Leica DFC350FXR2 digital camera mounted to the Leica microscope. The sample was observed through an oil immersion 63X/1.4 objective.

### Synthesis and characterization

Silicon nanoparticles (Si NPs) were prepared in inverse micelles using a modification of the method of Warner *et al.*<sup>5</sup> with a non-aggressive Si source, Si(OMe)<sub>4</sub>, and short sonication steps (30 min) instead of stirring (see Fig. 1). Alkylamine-terminated particles with three different alkyl chain lengths were obtained in the reactions of hydrogen-terminated Si NPs and propylamine, hex-5-enylamine and undex-10-en-1-amine, in the presence of a catalytic amount of H<sub>2</sub>PtCl<sub>6</sub>.

A typical TEM image of 3-aminopropyl-terminated Si NPs (Fig. 2) displays a particle size distribution of  $1.57 \pm 0.24$  nm,

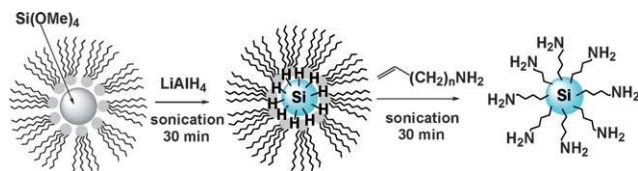


Fig. 1 Synthesis and functionalization of Si NPs ( $n = 1, 4, 9$ ).

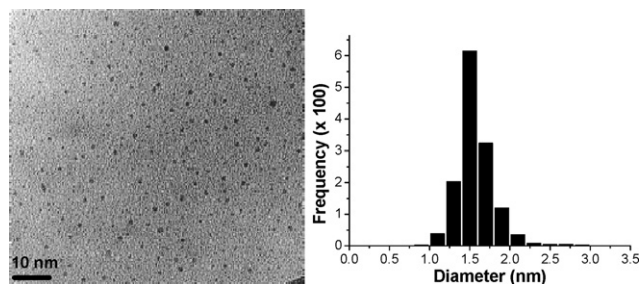
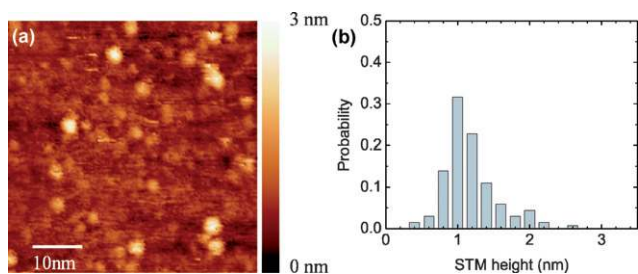


Fig. 2 TEM image of 3-aminopropyl-terminated Si NPs and corresponding particle size distribution histogram.



**Fig. 3** Large-scale STM image of: (a) 3-aminopropyl-terminated Si NPs on a Au(111) substrate. STM parameters  $V_{\text{bias}}$ : 2.5 V,  $I_{\text{set-point}}$ : 10 pA. (b) Histogram of Si NP heights extracted from the STM topography.

measured from 1365 NPs on different parts of the grid. This value and distribution of the size of the Si core (the alkyl chains do not show up in TEM) was independent of the alkyl spacer length, which excludes effects of the Si NP core size on their optical properties, and also shows that the method used to make such NPs is reproducible.

The Si NPs have been deposited on a Au(111) substrate and probed with UHV-STM. The topographic STM image (Fig. 3) also shows well-separated Si NPs that can be easily identified. The stable topography indicates that the Si NPs are anchored *via* Au–NH<sub>2</sub> bonds. From previous investigations performed on different types of nanocrystals,<sup>59</sup> it was shown that the size of the particles can be measured in the height profile obtained from the topographic images. In contrast, the lateral dimensions of the nanoparticle are generally larger due to tip convolution effects. A histogram of the height of the NPs measured from the topographic images is shown in Fig. 3b. The average STM height is around 1 nm, which is slightly smaller than the core diameter deduced from the TEM analysis (Fig. 2). This may reflect a combination of size and electronic effects (*i.e.* different density of states on bare Au and the Si NPs). However, the shape of STM height histogram completely resembles the TEM histogram.

## Determination of the band gap: optical absorption and scanning tunneling spectroscopy

All synthesized amine-terminated Si NPs show a broad continuous absorption between 200–450 nm (Fig. 4, top), *i.e.* with a clearly red-shifted absorption compared to alkyl-terminated Si NPs.<sup>6b</sup>

The absorption spectrum of 3-aminopropyl-terminated Si NPs has a distinctive broad peak at 300 nm and a less pronounced absorption around 265 nm. The disappearance of the most apparent peak/shoulder in the absorption spectra with increasing length of the alkyl spacer probably reflects the variation in the oxygen content at the NP surface, which has for alkyl-terminated Si NPs been shown to be linked to the length of the alkyl spacer.

Quantum chemical calculations predict that the presence of an NH<sub>2</sub> group in the vicinity of Si NPs results, for small NPs such as those being studied, in narrowing the energy gap (HOMO–LUMO gap).<sup>60</sup> When the length of the capping molecule is increased, the effect of narrowing the band gap is smaller, resulting in the blue shift of the absorption bands.

It should also be noted that with increasing alkyl chain length the obtained alkyl-terminated Si NPs are less oxidized

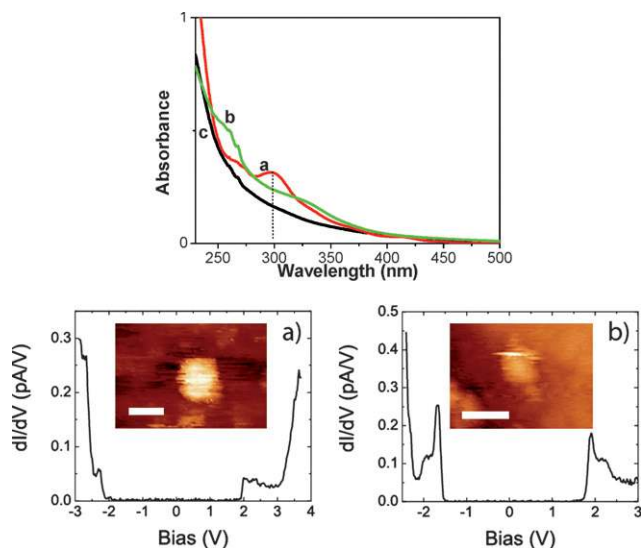


**Fig. 4** (Top) Absorption spectrum of (a) Si–C<sub>3</sub>H<sub>6</sub>NH<sub>2</sub>, (b) Si–C<sub>6</sub>H<sub>12</sub>NH<sub>2</sub> and (c) Si–C<sub>11</sub>H<sub>22</sub>NH<sub>2</sub> NPs. (Bottom) Spectroscopy on individual Si NPs. STS settings are  $V_{\text{bias}}$ : 3.6 V,  $I_{\text{set-point}}$ : 100 pA and  $V_{\text{bias}}$ : 3.0 V,  $I_{\text{set-point}}$ : 100 pA; 5 K. The spectra show a large zero-conductance gap in the range of 4 V with a strongly increasing local density of states (LDOS) at positive and negative bias. The scale bar represents 10 nm.

(noticeable *via* the Si–O bond in the IR spectra; not shown).<sup>6b</sup> Thus, beside a distance dependent on the influence of the amine groups to the Si core, a higher degree of oxidation can also contribute to red-shifted absorption.<sup>61</sup>

We have also studied the electronic spectra of individual Si NPs. Band gaps of individual Si NPs were measured by scanning tunneling spectroscopy (STS), and are in the 4–5 eV range for 60% of the measured NPs, and 3–3.75 eV for the rest.<sup>59,62</sup> On two identically prepared samples, 14 and 17 dots were investigated, respectively. Fig. 4a and 4b (bottom) show two measured conductance spectra on individual Si NPs. The spectra show resonances at positive (conduction levels) and negative bias (valence levels) separated by a large zero-conductance gap. Here we only focused on the STS spectra showing a large STS gap. This value is close to what is theoretically calculated for Si NPs with a Si core diameter of  $\sim 1$  nm.<sup>63</sup> Such a large band gap has also been seen in the optical spectroscopy (Fig. 4, top) and accurately corresponds to the most pronounced band at 300 nm.

## Luminescence spectra

Emission spectra of amine-terminated Si NPs are recorded upon various excitation wavelengths, from 280 to 460 nm. All the NPs being studied display an intense emission in the 350–600 nm range. The size dispersion is revealed in the luminescence data, where excitation with different wavelengths specifically causes the emission of Si NPs of different sizes. However, the emission spectra, and specifically the wavelength at which the maximum emission intensity is observed depends on the length of the alkyl spacer (Fig. 5). With a short (–C<sub>3</sub>H<sub>6</sub>) spacer the maximum emission is observed in the blue region at  $\lambda_{\text{em}}^{\text{max}} = 475$  nm, when exciting Si NPs at 390 nm. For longer chains the maximum emission gradually shifts to the UV: for the C<sub>6</sub>H<sub>12</sub>

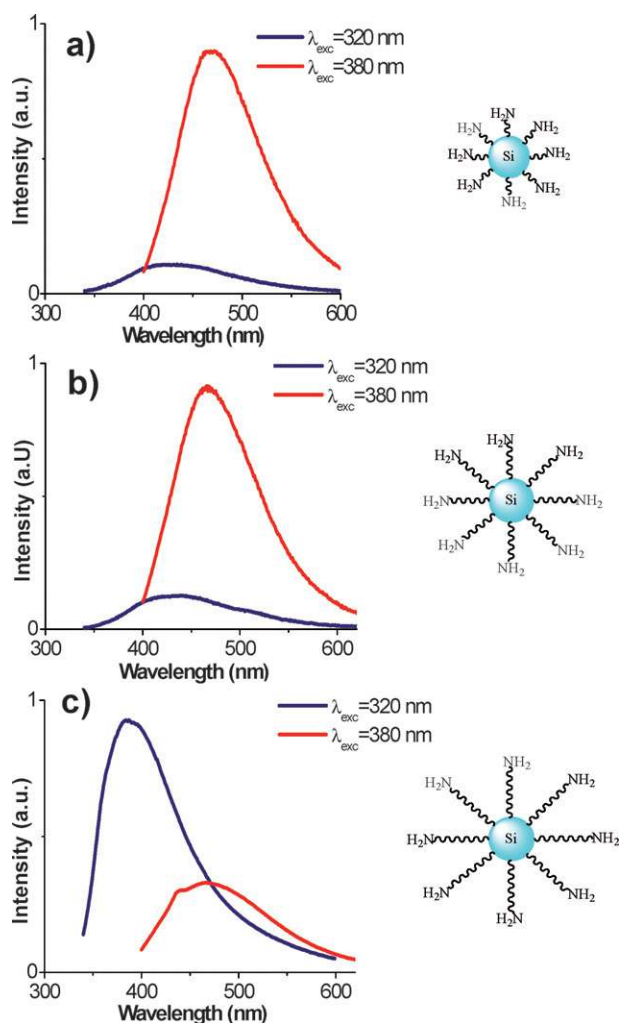


**Fig. 5** Dominant emission of 3-aminopropyl (a), 6-aminohexyl (b) and 11-aminoundecyl (c) terminated Si NPs in water. Note: Si NP core size is identical in all cases.

spacer  $\lambda_{\text{exc}}^{\text{max}} = 380$  nm and  $\lambda_{\text{em}}^{\text{max}} = 467$  nm; for the  $\text{C}_{11}\text{H}_{22}$  spacer  $\lambda_{\text{exc}}^{\text{max}} = 320$  nm, while  $\lambda_{\text{em}}^{\text{max}} = 385$  nm. These values can be compared to analogous features for alkyl-functionalized oxide-free Si NPs of the same size, which display  $\lambda_{\text{exc}}^{\text{max}} = 260$  nm and  $\lambda_{\text{em}} = 283$  nm.<sup>6b</sup> The longer the alkyl chain between the Si NPs core and amine moiety, the shorter the wavelength of maximum emission, and thus: the more the  $\text{NH}_2$ -terminated Si NPs resemble alkyl-terminated Si NPs. The positions of the emission maxima are almost identical for excitation wavelengths above 360 nm for all the synthesized Si NPs. However, upon excitation with light at 300–320 nm, maxima of the  $\text{Si-C}_{11}\text{H}_{22}\text{NH}_2$  NPs are blue-shifted by  $\sim 45$  nm ( $\sim 0.3$  eV) compared to what is observed for Si NPs with shorter chains (see Fig. 5).

In all cases, the luminescence is very broad and its energy falls between 2 and 3 eV. A large Stokes shift ( $\sim 1$  eV) and the broadness of the emission indicate that the observed luminescence is not a true band gap process. As previously mentioned, the exciton can be self-trapped or luminescence can occur *via* an energy level band gap.<sup>46</sup> Our results are in line with the change in passivation; attachment of shorter chains used for passivation of Si NPs is accompanied by a more oxidized NP surface and *vice*

*versa*.<sup>6b</sup> Therefore it is likely that Si NPs with shorter alkylamine chains have more trapped states. Electron-hole recombination then occurs *via* carriers trapped in oxygen-related localized states that become observable due to an increase of the band gap induced by quantum confinement. This effect is especially pronounced for ultrasmall Si NPs (1–2 nm), while for larger Si NPs ( $> 3$  nm) there is no broadening or red shift in emission, since the Si=O surface states are located outside the band gap.<sup>64</sup> So even though we cannot rule out the passivation effects we believe that a simple explanation of the observed behavior is not possible.

The quantum yields (QY) of photoluminescence of amine-terminated Si NPs were measured in water at pH = 7.5, and are displayed in Table 1. The fluorescence quantum efficiency is  $\sim 12\%$  and is comparable to the published quantum yields for wet-chemically prepared functionalized Si NPs,<sup>5,6b,19</sup> and independent of the chain length. So, while the energy of emission can be fine-tuned by the chain length, the overall efficiency is more or less independent.

All three types of Si NPs show similar lifetimes at  $\lambda_{\text{em}} = 450$  nm, which can be fitted as a three-exponential decay with lifetime contributions of 0.1 ns ( $\sim 10\%$ ), 0.9 ns (25–40%) and 4.5 ns (45–65%). Upon excitation of the NPs with 372 nm light, the overall decay time increases for longer emission wavelengths by an increase of the longest component from 4.2 to 4.9 ns (Fig. 6). This is likely to be caused by some dispersity in the Si core size, as the relaxation rates are likely to be size-dependent. Probing at longer emission wavelengths may, due to quantum confinement, shift the focus to larger NPs.

These short lifetimes ( $< 10$  ns) indicate a direct band gap emission of amine-terminated Si NPs.<sup>2</sup> If this would not be the case, lifetimes would be in the  $\mu\text{s}$  range.<sup>63</sup> Combining the obtained values for the fluorescence quantum yield and lifetimes,

**Table 1** Optical properties of amine-terminated Si NPs

	Emission maximum		FWHM		QY (%)
	$\lambda_{\text{exc}}/\text{nm}$	$\lambda_{\text{max}}/\text{nm}$	nm	eV	
$\text{Si-C}_3\text{H}_6\text{NH}_2$	390	475	98	0.53	$13.2 \pm 0.6$
$\text{Si-C}_6\text{H}_{12}\text{NH}_2$	380	467	100	0.56	$11.0 \pm 0.5$
$\text{Si-C}_{11}\text{H}_{22}\text{NH}_2$	320	385	98	0.77	$12.4 \pm 0.5$

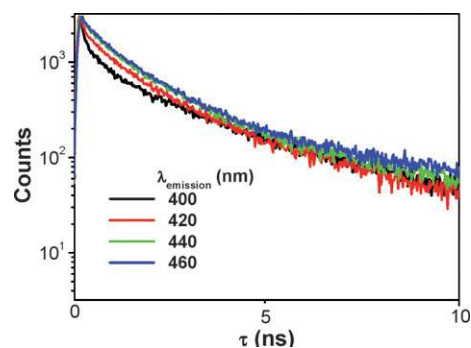


**Fig. 6** Fluorescence time-resolved decays at different emission wavelengths for 3-aminopropyl-terminated Si NPs in water,  $\lambda_{\text{exc}} = 372$  nm.

the overall decay rates can be calculated to be in the range  $0.6 \times 10^9$ – $4.4 \times 10^9 \text{ s}^{-1}$ ,<sup>65</sup> which is in line with a direct band gap excitation of the thus formed Si nanostructures.<sup>2</sup>

Since it is known that the amine moiety can strongly quench the emission of semiconductor quantum dots,<sup>47,48</sup> it was of interest to investigate this phenomenon with the amine-terminated Si NPs. This can be easily achieved *via* a variation of the pH, since this effectively transforms an  $-\text{NH}_2$  moiety with a lone electron pair, available for electron donation, into an  $-\text{NH}_3^+$  group that lacks this capability. With this aim, we obtained emission spectra at pH = 1.0, 7.5 and 13.3 (not shown), and observed that  $\lambda_{\text{em}}^{\text{max}}$  is independent of the pH, to within the experimental error of  $\sim 1 \text{ nm}$ . This surprising result implies that the emission of NPs with protonated (non-quencher) and non-protonated (quencher) amine groups originates from the same state. An effect of the pH on the emission intensity for Si NPs is observed (maximum changes of  $\sim 40\%$  for  $\text{C}_3\text{H}_6$  linker; smallest ( $\sim 10\%$ ) changes for  $\text{C}_{11}\text{H}_{22}$  chains): at lower pH the overall emission intensity is always higher, while—as said before—the energy of the emission maximum is unaffected.

Combined with the data shown in Fig. 5 the following picture arises: amine moieties can display some influence on the Si core, but there is only marginal electronic coupling (*i.e.* delocalization of HOMO and/or LUMO onto the  $\text{NH}_2$  groups). The excited states of the various alkylamine-terminated Si NPs are therefore more or less the same, only differing by the degree of oxidation that is slightly chain dependent. At low pH all amine groups are protonated, and electron transfer between the amine moieties and the Si core is precluded, yielding a higher emission intensity as observed. At higher pH protonation is either incomplete or absent, which allows involvement of the nitrogen lone pair in relaxation processes and yields a reduced emission and shorter excited state lifetime.

It has to be noted that the NPs remained highly stable also in these extremely acidic or basic conditions. Upon the exposure to pH = 1 at room temperature, the NPs remained chemically and photophysically stable even after several months! Perhaps even more surprising is that Si NPs also display tremendous resistance to a high pH of 13.3: the emission dropped only 5% after 10 h, and 38% after 150 h (Fig. 7, top). The lifetimes (Fig. 7, bottom) become somewhat shorter with increasing pH. This is not due to a change of the three components (0.1, 0.9 and 4.5 ns), but lowering the pH increases the 0.9 ns component at the cost of the 4.5 ns component. In other words, the pH dependence on both the overall emission and lifetime points to a quenching route for excited Si NPs that involves the N lone pair, but which is not the exclusive decay path. Importantly, IR measurements after storing the particles at pH = 13.3 for 6 h still indicate the presence of an aminoalkyl monolayer.

These observations indicate a very high degree of surface passivation by the amino-alkyl layer, and can be placed in context by noting that a planar Si surface that is coated with a covalently attached monolayer will typically lose that monolayer within 1 h at pH = 13. In other words, while NPs have a relatively large surface in comparison to their core, and are thus extremely prone to surface reactions—as is observed in the oxidation of H-terminated Si NPs<sup>64</sup>—the surface passivation of alkylamine-terminated Si NPs is good enough to withstand even these extreme conditions. Such coated NPs are also very stable

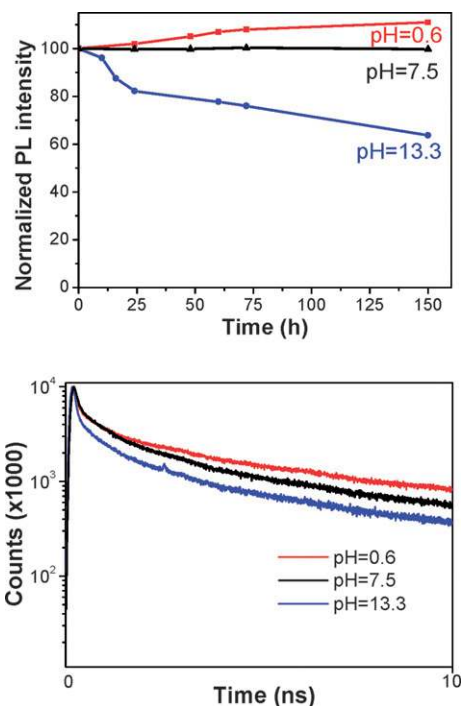


**Fig. 7** (Top) Change of 3-aminopropyl-terminated Si NPs emission intensity with time at different pH. (Bottom) Dependence of pH of the aqueous medium on the fluorescence lifetime of 3-aminopropyl-terminated Si NPs.

under sterilization conditions (121 °C, 30 min), which is highly relevant for any toxicology studies. The overall emission intensity remains unchanged after the exposure of the NPs to 121 °C for 30 min, while a slight peak broadening was observed (increase of full width at half maximum (FWHM) by 1–2 nm), probably due to some oxidation. This very long stability of the fluorescence in aqueous media is, of course, also highly beneficial for bioimaging studies (*vide infra*).

## Shape and diffusion of Si NPs

To determine the exact shape and possible aggregation of alkylamine-coated Si NPs, fluorescence anisotropy measurements were performed in solutions of different viscosities. All anisotropy decay curves could be fitted well with one-exponential functions, which implies that these NPs are monodisperse, and also that the shape of these NPs is spherical, as not obeying either of these conditions would have yielded multi-exponential fits.<sup>65</sup> In addition, it follows that aggregation of these NPs does not occur to any significant degree.

The viscosity dependence of the rotation correlation time of 3-aminopropyl Si NPs has been measured in the viscosity range of  $0.6 \times 10^{-3}$ – $6.2 \times 10^{-3} \text{ Pa s}$ . For this purpose NPs were dried and dissolved in different solvents: methanol, water and sucrose solutions in water (20–42%). Fig. 8 shows that this dependence is linear in the examined viscosity range, as expected for spherical bodies,<sup>65</sup> further confirming the ball shape of the NPs. From the slope of the line in Fig. 8 the diameter of the Si NPs can be determined to be  $1.6 \pm 0.1 \text{ nm}$ . This is in good agreement with the TEM data (Fig. 2), given the short and flexible  $(\text{CH}_2)_3\text{NH}_2$  chain.

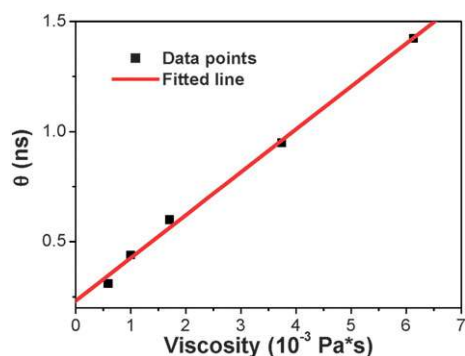


**Fig. 8** Dependence of the rotation correlation time ( $\theta$ ) on solvent viscosity for 3-aminopropyl Si NPs at constant temperature (298 K).

Fluorescence correlation spectroscopy was used to determine the mobility of Si NPs. The obtained diffusion times in water ( $\tau_D = 13.5 \mu\text{s}$ ) and in 25% sucrose solution in water ( $\tau_D = 33.8 \mu\text{s}$ ) allowed us to calculate the diffusion coefficient of Si NPs.<sup>66</sup> Their values are  $3.13 \times 10^{-10} \text{ m}^2 \text{ s}^{-1}$  in water, and  $1.25 \times 10^{-10} \text{ m}^2 \text{ s}^{-1}$  in 25% sucrose solution. By determining the diffusion time of the Si NPs in an exactly determined small volume, the size of the NPs could be derived—under assumption of a ball shape—to be  $1.4 \pm 0.3 \text{ nm}$ .<sup>67</sup> This size is in good agreement with the values obtained by TEM, STM, and the anisotropy decay measurements.

## Bioimaging

Finally, to study the potential for bioimaging of these water-soluble Si NPs, a murine cell line (BV2) has been stained with an aqueous solution of Si- $\text{C}_6\text{H}_{12}\text{NH}_2$  NPs. To examine the exact distribution of these Si NPs in the cells, a second experiment was performed in which cellular nuclei were first stained with commercially available DRAQ5, a far-red fluorescent DNA-staining dye, and subsequently exposed to an aqueous solution of these Si NPs. After incubation and centrifugation, the cells were observed consecutively with 488 and 543 nm excitation wavelengths.

From the images displayed in Fig. 9 it is clear that these Si NPs are readily taken up by BV2 nerve cells, are located in the cytosol and do not tend to relocate to the nuclei.

Due to the photostability of the Si NPs prolonged irradiation allowed us to follow the mitosis of the cells. Newly formed daughter cells are also being stained by Si NPs, and in this fashion it is possible to follow multiple generations of cells without further staining. As the cells keep on multiplying without

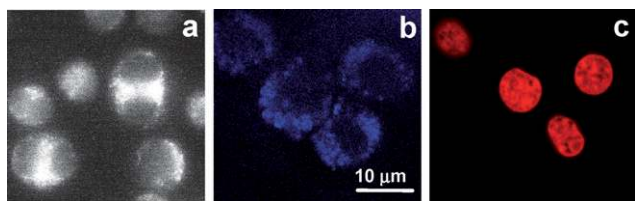


**Fig. 9** (a) Epifluorescence image of mitosis of BV2 cells stained with Si NPs under blue light irradiation (b) and (c) confocal image of BV2 cells simultaneously stained with Si NPs and DRAQ5.

noticeable changes in the proliferation rate, this strongly indicates the fact that these Si NPs are not noticeably toxic under these conditions in line with more detailed toxicological tests.<sup>7b</sup> This opens up a wide range of applications in biological studies.

## Conclusions

In conclusion, amine-terminated Si nanoparticles (NPs) with different linker lengths between the Si core and the  $\text{NH}_2$  moiety were successfully synthesized. The obtained NPs have a spherical shape, homogeneous size distribution and a very high mobility in water. The directly measured band gap by STS is in line with absorption data and is  $\sim 4 \text{ eV}$ . The maximum emission of Si NPs of the same core size and functionalization can be tuned in a controllable fashion from the UV to the blue spectral region, by simply changing the distance between the Si core and the amino group. These amine-terminated Si NPs show a great chemical and photophysical stability over a very wide pH range (1–13.3). Interestingly, the lifetimes of the NPs are shorter at higher pH (at which the N lone pair is available to interact with Si core), but the maximum of the emission is unaffected by the pH.

Si NPs are shown to be suitable candidates for *in vivo* labelling. Unchanged proliferation of stained BV2 cells was observed, which suggests a minimal toxicity under the conditions used. Daughter cells were still clearly stained with Si NPs, which makes it possible to follow stained multiple cell generations by simply staining the first generation of cells. Determination of the maximum concentration of Si NPs that can be used for multi-generation staining and detailed studies of the effects on different cell types are currently ongoing in our labs.

## Acknowledgements

We thank Benedikt Gralla (Physikalisches Institut, Univ. of Münster) for help with TEM measurements, Adrie H. Westphal (Wageningen University) for conducting FCS measurements, and NanoNed, funded by the Dutch Ministry of Economic Affairs (project WOE.7713), for financial support.

## References

- 1 G. Belomoin, J. Therrien, A. Smith, S. Rao, R. Twesten, S. Chaieb, M. H. Nayfeh, L. Wagner and L. Mitas, *Appl. Phys. Lett.*, 2002, **80**, 841–843.
- 2 D. S. English, L. E. Pell, Z. H. Yu, P. F. Barbara and B. A. Korgel, *Nano Lett.*, 2002, **2**, 681–685.
- 3 S. Schuppler, S. L. Friedman, M. A. Marcus, D. L. Adler, Y. H. Xie, F. M. Ross, Y. J. Chabal, T. D. Harris, L. E. Brus, W. L. Brown, E. E. Chaban, P. F. Szajowski, S. B. Christman and P. H. Citrin, *Phys. Rev. B*, 1995, **52**, 4910–4925.
- 4 E. Rogozhina, G. Belomoin, A. Smith, L. Abuhassan, N. Barry, O. Akcikir, P. V. Braun and M. H. Nayfeh, *Appl. Phys. Lett.*, 2001, **78**, 3711–3713.
- 5 J. H. Warner, A. Hoshino, K. Yamamoto and R. D. Tilley, *Angew. Chem., Int. Ed.*, 2005, **44**, 4550–4554.
- 6 (a) J. Zou, R. K. Baldwin, K. A. Pettigrew and S. M. Kauzlarich, *Nano Lett.*, 2004, **4**, 1181–1186; (b) M. Rosso-Vasic, E. Spruijt, B. van Lagen, L. De Cola and H. Zuilhof, *Small*, 2008, **4**, 1835.
- 7 (a) A. H. Mayne, S. C. Bayliss, P. Barr, M. Tobin and L. D. Buckberry, *Phys. Status Solidi A*, 2000, **182**, 505–513; (b) L. Ruizendaal, S. Bhattacharjee, K. Pournazari, M. Rosso-Vasic, L. H. J. de Haan, G. M. Alink, A. T. M. Marcelis and H. Zuilhof, *submitted*.

- 8 C. Kirchner, T. Liedl, S. Kudera, T. Pellegrino, A. M. Javier, H. E. Gaub, S. Stolze, N. Fertig and W. J. Parak, *Nano Lett.*, 2005, **5**, 331–338.
- 9 J. R. Nilsson, *Acta Protozool.*, 2003, **42**, 19–29.
- 10 Y. B. Zhang, W. Chen, J. Zhang, J. Liu, G. P. Chen and C. Pope, *J. Nanosci. Nanotech.*, 2007, **7**, 497–503.
- 11 D. A. B. Miller, *Nature*, 1995, **378**, 238–238.
- 12 H. L. Zhang, T. C. Liu, J. H. Wang, Z. L. Huang, Y. D. Zhao and Q. M. Luo, *Chin. J. Anal. Chem.*, 2006, **34**, 1491–1495.
- 13 Y. Zhong, N. Kaji, M. Tokeshi and Y. Baba, *Expert Rev. Proteomics*, 2007, **4**, 565–572.
- 14 J. L. Heinrich, C. L. Curtis, G. M. Credo, K. L. Kavanagh and M. J. Sailor, *Science*, 1992, **255**, 66–68.
- 15 F. J. Hua, F. Erogbogbo, M. T. Swihart and E. Ruckenstein, *Langmuir*, 2006, **22**, 4363–4370.
- 16 F. J. Hua, M. T. Swihart and E. Ruckenstein, *Langmuir*, 2005, **21**, 6054–6062.
- 17 X. Li, Y. He and M. T. Swihart, *Langmuir*, 2004, **20**, 4720–4727.
- 18 X. Li, Y. He, S. S. Talukdar and M. T. Swihart, *Langmuir*, 2003, **19**, 8490–8496.
- 19 J. D. Holmes, K. J. Ziegler, R. C. Doty, L. E. Pell, K. P. Johnston and B. A. Korgel, *J. Am. Chem. Soc.*, 2001, **123**, 3743–3748.
- 20 Q. Liu and S. M. Kauzlarich, *Mater. Sci. Eng.*, 2002, **B96**, 72–75.
- 21 K. A. Pettigrew, Q. Liu, P. P. Power and S. M. Kauzlarich, *Chem. Mater.*, 2003, **15**, 4005–4011.
- 22 X. Zhang, D. Neiner, S. Wang, A. Y. Louie and S. M. Kauzlarich, *Nanotechnology*, 2007, **18**, 095601–095606.
- 23 D. Neiner, H. W. Chiu and S. M. Kauzlarich, *J. Am. Chem. Soc.*, 2006, **128**, 11016–11017.
- 24 J. Zou, P. Sanelle, K. A. Pettigrew and S. M. Kauzlarich, *J. Cluster Sci.*, 2006, **17**, 565–578.
- 25 J. P. Wilcoxon and G. A. Samara, *Appl. Phys. Lett.*, 1999, **74**, 3164–3166.
- 26 J. P. Wilcoxon, G. A. Samara and P. N. Provencio, *Phys. Rev. B*, 1999, **60**, 2704–2714.
- 27 R. D. Tilley, J. H. Warner, K. Yamamoto, I. Matsui and H. Fujimori, *Chem. Commun.*, 2005, 1833–1835.
- 28 D. Mayeri, B. L. Phillips, M. P. Augustine and S. M. Kauzlarich, *Chem. Mater.*, 2001, **13**, 765–770.
- 29 E. V. Rogozhina, D. A. Eckhoff, E. Gratton and P. V. Braun, *J. Mater. Chem.*, 2006, **16**, 1421–1430.
- 30 S. Sato and M. T. Swihart, *Chem. Mater.*, 2006, **18**, 4083–4088.
- 31 A. Saár, Y. Reichman, M. Dovrat, D. Krapf, J. Jedrzejewski and I. Balberg, *Nano Lett.*, 2005, **5**, 2443–2447.
- 32 J. G. C. Veinot, *Chem. Commun.*, 2006, 4160–4168.
- 33 (a) Photochemical: Q.-Y. Sun, L. C. P. M. de Smet, B. Van Lagen, M. Giesbers, P. C. Thuene, J. Van Engelenburg, F. A. De Wolf, H. Zuilhof and E. J. R. Sudholter, *J. Am. Chem. Soc.*, 2005, **127**, 2514–2523; (b) Thermal: A. B. Sieval, V. Vleeming, H. Zuilhof and E. J. R. Sudholter, *Langmuir*, 1999, **15**, 8288–8291.
- 34 (a) E. G. Stewart, T. W. Geders, M. J. Allen, H. C. Choi and J. M. Buriak, *Phys. Status Solidi A: Appl. Res.*, 2000, **182**, 109–115; (b) J. M. Buriak, M. P. Stewart, T. W. Geders, M. J. Allen, H. C. Choi, J. Smith, D. Raftery and L. T. Canham, *J. Am. Chem. Soc.*, 1999, **121**, 11491–11502; (c) J. M. Buriak, *Adv. Mater.*, 1999, **11**, 265–267.
- 35 L. Scheres, A. Arafat and H. Zuilhof, *Langmuir*, 2007, **23**, 8343–8346.
- 36 A. B. Sieval, A. L. Demirel, J. W. M. Nissink, M. R. Linford, J. H. van der Maas, W. H. de Jeu, H. Zuilhof and E. J. R. Sudholter, *Langmuir*, 1998, **14**, 1759–1768.
- 37 J. M. Buriak, *Chem. Rev.*, 2002, **102**, 1271–1308.
- 38 L. C. P. M. de Smet, A. V. Pukin, Q.-Y. Sun, B. J. Eves, G. P. Lopinski, G. M. Visser, H. Zuilhof and E. J. R. Sudholter, *Appl. Surf. Sci.*, 2005, **252**, 24–30.
- 39 L. Scheres, R. Achten, M. Giesbers, L. C. P. M. de Smet, A. Arafat, E. J. R. Sudholter, A. T. M. Marcelis and H. Zuilhof, *Langmuir*, 2009, **25**, 1529–1533.
- 40 Q.-Y. Sun, L. C. P. M. de Smet, B. van Lagen, A. Wright, H. Zuilhof and E. J. R. Sudholter, *Angew. Chem., Int. Ed.*, 2004, **43**, 1352–1355.
- 41 M. Rosso-Vasic, L. De Cola and H. Zuilhof, *J. Phys. Chem. C*, 2009, **113**, 2235–2240.
- 42 J. Nelles, D. Sendor, A. Ebbers, F. M. Petrat, H. Wiggers, C. Schulz and U. Simon, *Colloid Polym. Sci.*, 2007, **285**, 729–736.
- 43 L. T. Canham, *Appl. Phys. Lett.*, 1990, **57**, 1046–1048.
- 44 K. Matsumoto, M. Inada, I. Umezumi and A. Sugimura, *Jpn. J. Appl. Phys.*, 2005, **44**, 8742–8746.
- 45 D. Bisero, F. Comi, C. Nobili, R. Tonini, G. Ottaviani, C. Mazzoleni and L. Pavesi, *Appl. Phys. Lett.*, 1995, **67**, 3447–3449.
- 46 S. Godefroo, M. Hayne, M. Jivanescu, A. Stesmans, M. Zacharias, O. I. Lebedev, G. Van Tendeloo and V. V. Moshchalkov, *Nat. Nanotechnol.*, 2008, **3**, 174–178.
- 47 C. Landes, C. Burda, M. Braun and M. A. El-Sayed, *J. Phys. Chem. B*, 2001, **105**, 2981–2986.
- 48 C. F. Landes, M. Braun and M. A. El-Sayed, *J. Phys. Chem. B*, 2001, **105**, 10554–10558.
- 49 M. Bruchez, M. Moronne, P. Gin, S. Weiss and A. P. Alivisatos, *Science*, 1998, **281**, 2013–2016.
- 50 X. Michalet, F. F. Pinaud, L. A. Bentolila, J. M. Tsay, S. Doose, J. J. Li, G. Sundaresan, A. M. Wu, S. S. Gambhir and S. Weiss, *Science*, 2005, **307**, 538–544.
- 51 F. Pinaud, X. Michalet, L. A. Bentolila, J. M. Tsay, S. Doose, J. J. Li, G. Iyer and S. Weiss, *Biomaterials*, 2006, **27**, 1679–1687.
- 52 P. Alivisatos, *Nat. Biotechnol.*, 2004, **22**, 47–52.
- 53 X. Michalet, F. Pinaud, T. D. Lacoste, M. Dahan, M. P. Bruchez, A. P. Alivisatos and S. Weiss, *Single Mol.*, 2001, **2**, 261–276.
- 54 D. Gerion, F. Pinaud, S. C. Williams, W. J. Parak, D. Zanchet, S. Weiss and A. P. Alivisatos, *J. Phys. Chem. B*, 2001, **105**, 8861–8871.
- 55 B. O. Dabbousi, J. RodriguezViejo, F. V. Mikulec, J. R. Heine, H. Mattoussi, R. Ober, K. F. Jensen and M. G. Bawendi, *J. Phys. Chem. B*, 1997, **101**, 9463–9475.
- 56 Z. F. Li and E. Ruckenstein, *Nano Lett.*, 2004, **4**, 1463–1467.
- 57 L. Jdira, P. Liljeroth, E. Stoffels, D. Vanmaekelbergh and S. Speller, *Phys. Rev. B*, 2006, **73**, 115305–115311.
- 58 A. T. R. Williams, S. A. Winfield and J. N. Miller, *Analyst*, 1983, **108**, 1067–1071.
- 59 P. Liljeroth, P. A. Z. van Emmichoven, S. G. Hickey, H. Weller, B. Grandidier, G. Allan and D. Vanmaekelbergh, *Phys. Rev. Lett.*, 2005, **95**, 086801–086807.
- 60 X. Wang, R. Q. Zhang, T. A. Niehaus and T. Frauenheim, *J. Phys. Chem. C*, 2007, **111**, 2394–2400.
- 61 Z. Y. Zhou, L. Brus and R. Friesner, *Nano Lett.*, 2003, **3**, 163–167.
- 62 A. Franceschetti and A. Zunger, *Phys. Rev. B*, 2000, **62**, 2614–2623.
- 63 M. V. Wolkin, J. Jorne, P. M. Fauchet, G. Allan and C. Delerue, *Phys. Rev. Lett.*, 1999, **82**, 197–200.
- 64 D. A. MacLaren, N. J. Curson, P. Atkinson and W. Allison, *Surf. Sci.*, 2001, **490**, 285–295.
- 65 J. R. Lakowicz, *Principles of Fluorescence Spectroscopy*, Springer, 3rd edn, 2006.
- 66 V. Vukojevic, A. Pramanik, T. Yakovleva, R. Rigler, L. Terenius and G. Bakalkin, *Cell. Mol. Life Sci.*, 2005, **62**, 535–550.
- 67 P. D. Zhang, L. A. Li, C. Q. Dong, H. F. Qian and J. C. Ren, *Anal. Chim. Acta*, 2005, **546**, 46–51.